Numerical simulation of the breakup of a round liquid jet by a coaxial flow of gas with a subgrid Lagrangian breakup model

By D. Kim AND P. Moin

1. Motivation and objectives

One of the challenging problems in computational physics is to devise an integrated simulation of multiscale and multiphysics phenomena commonly found in nature. One important example is the multiphase phenomenon typically encountered in gas-turbine engines or internal combustion engines. Combustion of liquid fuels involves various physical processes such as liquid film atomization into droplet, evaporation, and turbulent mixing with the ambient gas when the combustion occurs. The atomization of a liquid film or jet can be divided into two subsequent processes: i.e., primary atomization followed by secondary atomization. The primary atomization is the initial breakup of the liquid jet into large and small liquid structures close to the injection nozzle. It involves complex interface topology of large coherent liquid structures. The secondary atomization is the subsequent breakup into smaller drops forming sprays. As distinct physical processes are involved in each regime, different modeling strategies are needed. The objective in the present study is to apply an appropriate physical model that captures each flow regime and to integrate the resulting model into a computational simulation of the whole combustion process.

The primary atomization is dominated by the interaction of the liquid film with the surrounding gas phase, giving rise to liquid surface instability waves. These interfacial instabilities are important in the overall spray evolution and droplet formation process. However, the dynamics of the phase interface is highly complex, poorly understood, and remains an unresolved problem in the area of atomization simulation. Atomization simulation is generally performed based on Lagrangian particle tracking and secondary breakup mechanisms, assuming that the typical size of the liquid drops is much smaller than the available grid resolution and that the shapes of the individual drops are similar to spheres or ellipsoids (Reitz 1987; Tanner 2004; Apte *et al.* 2003). Although these models can successfully predict secondary breakup, they are not applicable to the primary breakup regime because their underlying assumptions do not hold for the primary breakup regime where the length scale is an order of injector nozzle size.

In the primary breakup regime, the liquid fluid interacts with the surrounding turbulent gas phase, which results in complex topological shapes of the interface. The large-scale coherent structures that interact with the gas phase will disintegrate into filaments and breakup into droplets. Thus, if we are to capture the physical process that occurs at the phase interface, it must first be identified and tracked. To this end, the level set method coupled to the Navier-Stokes equation is employed in the present study. In order to correctly capture the breakup phenomenon of phase interface, the smallest length scale of the phase interface should be larger than the grid size in the level set grid. This results in severe grid requirement in numerical simulations because the range of the length scales

is from meters to micro-meters in real applications. Thus, an appropriate subgrid model has been developed to predict the breakup phenomenon occurring in the subgrid scales.

The secondary breakup is the subsequent breakup of liquid blobs or sheets into smaller droplets, generating vast number of atomized droplets. Thus, it becomes prohibitively expensive to resolve every droplet by the level-set interface tracking method used in the primary breakup regime. Instead, the Lagrangian particle tracking method is used to capture small-scale liquid droplets. The liquid particle motion is then simulated using Basset-Boussinesq-Oseen (BBO) equations (Crowe *et al.* 1998). It is assumed that the density of the particle is much larger than that of the gaseous fluid (O[1000]), that the particle size is small compared with the turbulence integral length scale, and that the effect of shear on the particle motion is negligible. The large density ratio means that the Basset force and the added mass term are small and, therefore, are neglected. Under these assumptions, the particle motion is governed by the Lagrangian equations. The further breakup of liquid drops into smaller drops is modeled by a stochastic breakup model, in which the characteristic radius of drops is assumed to be a time-dependent stochastic variable with a given initial-size distribution (Apte *et al.* 2003).

In the present study, a primary atomization is modeled by using the level set method to track the phase interface, whereas the Lagrangian tracking method with stochastic breakup is used to track subgrid droplets and its further secondary breakup. The subgrid Lagrangian breakup model is developed here to couple the level set method to Lagrangian tracking method, which plays an important role as a bridge to connect the primary atomization to secondary atomization. This numerical methodology enables us to simulate the whole breakup process.

2. Level set method

2.1. *Governing equations*

The Navier-Stokes equations for incompressible, immiscible, two-phase flow are described as

$$\frac{\partial \rho \mathbf{u}}{\partial t} + \nabla \cdot \rho \mathbf{u}\mathbf{u} = -\nabla \mathbf{p} + \nabla \cdot \tau + \mathbf{T}_\sigma \tag{2.1}$$

$$\nabla \cdot \mathbf{u} = \mathbf{0}, \tag{2.2}$$

where ρ is the density, p the pressure, τ the viscous stress tensor, and $\mathbf{T}_\sigma$ is the surface tension force.

A level set method is applied to track the location of the phase interface. The location and time evolution of the phase interface are described by the level set equation:

$$\frac{\partial G}{\partial t} + \mathbf{u} \cdot \nabla G = 0, \tag{2.3}$$

where the iso-surface $G = 0$ defines the location of the interface, $G > 0$ in the liquid, and $G < 0$ in the gas phase. In the computational domain, G is set to be a signed distance function to the interface:

$$|\nabla G| = 1. \tag{2.4}$$

The interface normal vector $\mathbf{n}$ and the interface curvature κ can be calculated as

$$\mathbf{n} = \frac{\nabla G}{|\nabla G|}, \tag{2.5}$$

$$\kappa = \nabla \cdot \mathbf{n}. \tag{2.6}$$

In this paper, we used the RLSG (Refined Level Set Grid) method (Herrmann 2008) to solve the coupled level set equations (2.3, 2.4). The level set transport Eq. (2.3) is solved on a separate refined G-grid using fifth-order WENO scheme (Jiang & Peng 2000) with a third-order TVD Runge-Kutta time discretization (Shu & Osher 1989). It is coupled to the flow solver through $\mathbf{u}$. The velocity $\mathbf{u}$ on the fine G-grid is obtained by trilinear interpolation from the flow solver grid. Reinitialization (2.4) is solved by an iterative procedure using a fifth-order WENO scheme and a first-order pseudo-time integration (Sussmann *et al.* 1994; Peng *et al.* 1999). The numerical details about the RLSG method are described in Herrmann (2008).

In order to solve the flow field, an unstructured grid solver (Mahesh *et al.* 2004; Ham & Iaccarino 2004; Herrmann 2008) is used based on a conservative formulation of the variable density Navier-Stokes equations (Pierce & Moin 2001; Kim & Moin 2011). The Navier-Stokes equations are coupled to the level set equation through the density, viscosity, and surface tension force. The density ρ and the viscosity μ in a cell i are defined as volume averaged quantities:

$$\rho_i = \psi_i \rho_l + (1 - \psi_i)\rho_g \tag{2.7}$$

$$\mu_i = \psi_i \mu_l + (1 - \psi_i)\mu_g, \tag{2.8}$$

where the subscript l denotes quantities in the liquid and the subscript g denotes those in the gas phase. The flow solver volume fraction ψ is defined as

$$\psi_i = \frac{1}{V_i} \int_{V_i} H(G) dV, \tag{2.9}$$

where H is the Heaviside function and V_i is the control volume of the flow solver grid cell. In the RLSG method, this integral is calculated on the G-grid as

$$\frac{1}{V_i} \int_{V_i} H(G) dV = \frac{\sum_{i_G} \psi_{i_G} V_{i,i_G}}{\sum_{i_G} V_{i,i_G}} \tag{2.10}$$

where V_{i,i_G} is the joined intersection volume of the G-grid cell i_G and the flow solver control volume V_i, and the G-grid volume fraction ψ_{i_G} is calculated using an analytical formula developed by van der Pijl *et al.* (2005),

$$\psi_{i_G} = f(G_{i_G}, \mathbf{n}_{i_G}). \tag{2.11}$$

The surface tension force $\mathbf{T}_\sigma$ is calculated as

$$\mathbf{T}_{\sigma,i} = \int_{V_i} \sigma \kappa \nabla \psi d\mathbf{x}, \tag{2.12}$$

where σ is the surface tension force coefficient. The curvature κ is transferred from the G-grid to the flow solver grid,

$$\kappa = \frac{\sum_{i_G} V_{i,i_G} \delta_{i_G} \kappa_{i_G}}{\sum_{i_G} V_{i,i_G} \delta_{i_G}}, \tag{2.13}$$

where $\delta_{i_G} = 0$ if $\psi_{i_G} = 0$ or $\psi_{i_G} = 1$, and $\delta_{i_G} = 1$ otherwise. The details about the balanced force algorithm and curvature are described in Herrmann (2006).

3. Coupling level set to Lagrangian drop

3.1. *Broken-off drop transfer*

Two different numerical approaches are employed for primary and secondary atomization regimes. The level set method is used to track the large-scale dynamics of the phase interface ($l/\Delta x > 1$). On the other hand, the Lagrangian drop tracking method with stochastic breakup model is applied to secondary atomization regime where the drop sizes are smaller than the flow solver grid size ($l/\Delta x < 1$).

In order to couple the Lagrangian drop tracking method to the level set method, subgrid liquid droplets having spherical shape must be identified first. Then, they are removed from the level-set representation and inserted as liquid droplets that are tracked by the Lagrangian method if their volume is less than the volume of the local flow solver grid cell V_{cv} (see Fig. 1). The identification process can be easily done since the RLSG method can provide subgrid resolution with respect to the flow solver grid.

In order to identify broken-off drops, there are two criteria. The first one states that the drop volume V_D has to be smaller than the characteristic volume of flow-solver volume,

$$V_D \leq \gamma V_{cv}, \tag{3.1}$$

where V_{cv} is the volume of local flow solver grid cell volume. Here, the parameter γ is determined based on the size of flow-solver grid and the level-set grid. γ is set to 2 in the present simulations.

The second criterion regards shape. Although a broken-off liquid structure might satisfy the above volume criterion, it should not be transferred to the Lagrangian drop breakup model if its shape is not spherical, i.e., a thin ligament. The spherical shape criterion is defined as

$$r_{max} < \alpha r_{sphere}, \tag{3.2}$$

where r_{max} is the maximum distance between the center of mass and the surface of the drop and r_{sphere} is the radius of a corresponding sphere such that $4/3\pi r_{sphere}^3 = V_D$. Here, the parameter α is set to 2. If both criteria are satisfied, the liquid drop is removed from the level-set field by setting the G value of all cells of the broken drop to $-G$. Then its center of mass and total mass are inserted as the Lagrangian drop in the flow solver. Note that the transfer also conserves the momentum of the broken-off liquid droplet. This is one-way coupling between the level-set representation and Lagrangian drop. Once the broken-off droplets are transferred to Lagrangian drops, they do not turn back to the level-set representation.

4. Subgrid capillary breakup model for thin filament

4.1. *Pinching off of thin filament*

In the previous section, the small spherical drops produced through breakup process are transferred to Lagrangian drops. When the G-grid size is larger than the physical breakup length scale (ξ_b), however, thin structures are not resolved by the G grid and their mass is lost. The significant mass loss is inevitable if the G-grid size is larger than ξ_b because

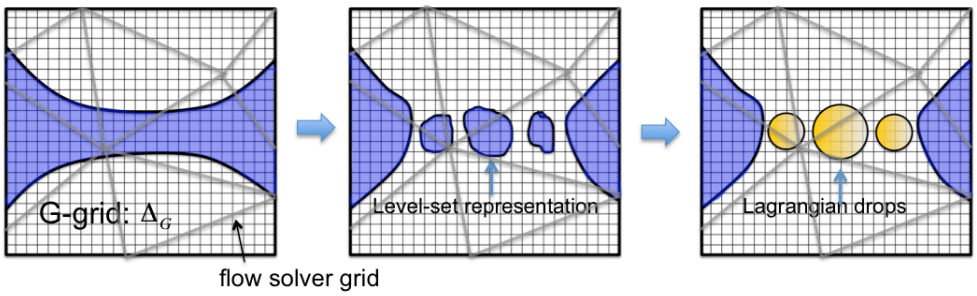

FIGURE 1. Subgrid broken-off drops in the level-set representation are identified and replaced with the Lagrangian drops having same mass and momentum.

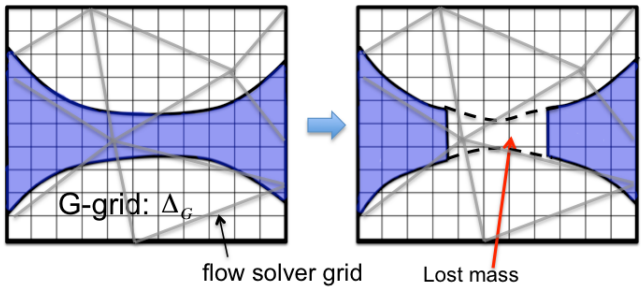

FIGURE 2. The artificial breakup of thin filament filament when $\Delta_G > \xi_b$.

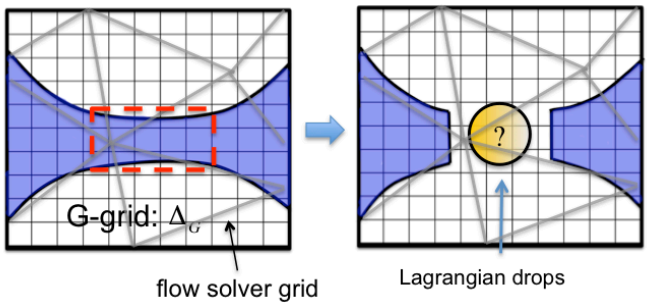

FIGURE 3. Subgrid filament structure is identified and replaced with Lagrangian drops having same mass.

representation of the interface on a discrete grid by an isosurface of a single scalar implies that any two interface segments approaching each other cannot be supported by the grid. When this happens, the mass between the two interfaces, where no node exists, is lost in the process (see Fig. 2). This artificial breakup happens when $\Delta_G > \xi_b$, which yields a significant amount of mass loss in simulations that contain many topology changes, as is the case in atomization. Thus, the G grid size should be smaller than breakup length scale ξ_b, otherwise the smallest drop size is dependent on the smallest G-grid size.

4.2. *Subgrid filament structure identification*

The thin filament structure smaller than the grid resolution must be identified and replaced with Lagrangian drops before losing its mass. In this section, the identification algorithm is discussed. The Lagrangian drop transfer algorithm is discussed in the next section. In order to identify thin filament structure before the numerical breakup, a numerical breakup length scale ($\alpha\Delta_G$) larger than the local grid size should be introduced in the level set method as

$$\lambda = \alpha\Delta_G, \tag{4.1}$$

with $\alpha > 1$. The thin filament identifying algorithm is

(a) Detect all interface cells (i) with $G > 0$ directly adjacent to $G = 0$.

(b) For the interface cells i, count the number of cells p in $\boldsymbol{n}_i$ direction until $G < 0$ or $p > \alpha$, where $\boldsymbol{n}_i = \nabla G/|\nabla G|$.

(c) If $p < \alpha$, tag all traversed cells and identify the interface cell e located at the end of the traversed cells. Then, calculate the contraction parameter defined as

$$C_r = (\boldsymbol{u}_i \cdot \boldsymbol{n}_i + \boldsymbol{u}_e \cdot \boldsymbol{n}_e), \tag{4.2}$$

where $\boldsymbol{u}_i$, $\boldsymbol{n}_i$ and $\boldsymbol{u}_e$, $\boldsymbol{n}_e$ are the velocities and normal vectors to the interface at the i and e cells, respectively.

(d) If $C_r > 0$, mark all contiguously tagged cells. These identified cells will be replaced by Lagrangian drops.

Here, α is usually set to 6 in the present simulations. Note that the thin filament identification reduces the effective G-grid resolution by a factor of α. Once the liquid filament region is identified, its volume can be calculated as in the broken-off drop case. However, the size and number of drops after breakup are unknown. Herrmann (2005) replaced the liquid region with one Lagrangian drop per processor in a parallel calculation for simplicity. In the present study, the Lagrangian drop-size distribution is predicted from the capillary instability theory explained in the following section.

4.3. *Capillary breakup model*

The breakup theory of thin liquid filament is a classical problem in fluid mechanics. Breakup yields an array of uniformly spaced large droplets with smaller droplets between them, known as satellite drops. Rayleigh (1878) studied the instability and breakup in the context of jets with inviscid assumption. Linear stability theory (Rayleigh 1878) can predict the initial disturbance growth rate, the time for breakup and the size of the mother drops. Linear theory, however, fails to capture the satellite drops because they are produced by a nonlinear interaction. Rayleigh's linearized analysis neglects the nonlinear terms and assumes a sinusoidal disturbance which remains sinusoidal during growth of the disturbance. Thus, breakup is assumed to occur only at the midpoint between two mother drops and small satellite drops are not predicted. In order to describe the nonlinear behavior and predict the satellite drops, higher-order nonlinear terms should be included in the analysis. Yuen (1968) showed that secondary waves are formed between the crests of the primary disturbance waves. These secondary waves result from the energy transfer from the primary waves through the higher order terms. The sizes of mother and satellite drops are predicted from the wavelength of the primary and secondary disturbances, respectively.

In the present study, the stability theory by Yuen (1968) is applied to predict the size of the mother and satellite drops, which is then be used to calculate the number and size of Lagrangian droplets in section 4.1.

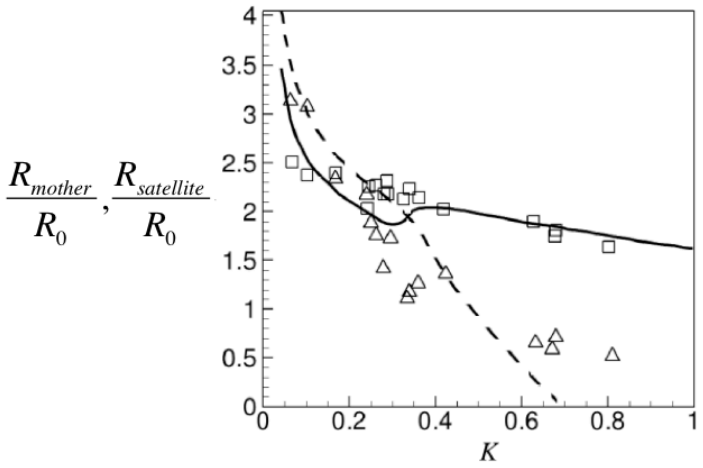

FIGURE 4. Predicted drop sizes and measured drop sizes from the experiment of water jets (Rutland & Jameson 1970): ——, predicted mother drop size; – – –, predicted satellite drop size; □ , measured mother drop size; △, measured satellite drop size.

By assuming an axisymmetric circular column of liquid jet with no outer gas, the disturbance on the interface can be expressed as a series expansion (Yuen 1968):

$$\eta(z,t) = \sum_{m=1}^{\infty} \eta_0^m \eta_m, \tag{4.3}$$

where $\eta(z,t)$ is the function for the interface location and z is the component in the axial direction. Here, η_0 is the initial perturbation given by $\eta_0 = 1 + \epsilon_0$, where ϵ_0 is the amplitude of the initial disturbance. $\eta(z,t)$ and η_0 are nondimensionalized by the initial jet radius R_0. The third-order solution ($m = 3$) of Eq. 4.3 for an axisymmetric incompressible inviscid Navier-Stokes equation is explicitly given as

$$\begin{aligned}\eta = {} & \eta_0 \cos Kz \cosh \omega_1 t \\ & + \eta_0^2 \Big(B_{22}(t) \cos 2Kz - \frac{1}{8}(\cosh \omega_1 t + 1) \Big) \\ & + \eta_0^2 \Big(B_{31}(t) \cos Kz + B_{33}(t) \cos 3Kz \Big),\end{aligned} \tag{4.4}$$

where K is the wave number nondimensionalized by R_0 and t is the dimensionless time with respect to $(R_0^3 \rho/\sigma)^{1/2}$. Here, σ is the surface tension coefficient. The coefficients B_{22}, B_{31} and B_{33} are given in Yuen (1968). Using Eq. 4.4, the wave profiles are calculated in time for a given wave number K. The breakup occurs when the wave reaches the centerline of the jet. The mother drop corresponds to the liquid region enclosed by the primary wave crest, and the satellite drop is formed under the secondary wave. Fig. 4 shows the size of mother and satellite drops for different wave numbers as well as the experimental data in the water jet experiment (Rutland & Jameson 1970). There is a good agreement between the experiments and the theoretical prediction at high and low wave numbers. From the linear analysis by citeRayleigh1878 for inviscid jets, the most unstable wave number is $K_{linear} = 0.697$. For this wave number, the ratio of the satellite

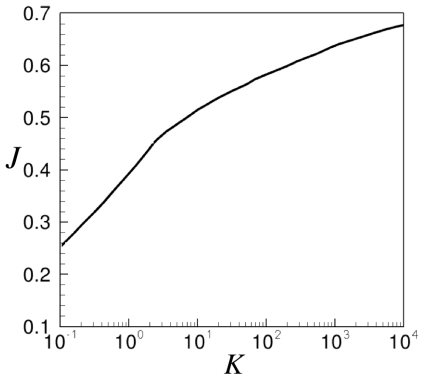

FIGURE 5. The most unstable wave number with respect to $J = \sigma R_0/\rho\nu^2$ (Chandrasekhar 1981).

drop size to the mother drop size is $R_{satellite}/R_{mother} = 0.01$. With viscous jets, however, the most unstable wave number depends on the parameter $J = \sigma R_0/\rho\nu^2$, which can be calculated by the full linearized theory (Chandrasekhar 1981), as shown in Fig. 5. In the case of an inviscid jet ($J \to \infty$) where the surface tension dominates over the viscous force, the most unstable wave number converges to $K_{linear} = 0.697$.

Once the most unstable wave number is calculated from the theory (Chandrasekhar 1981), the drop size ratio, $R_{satellite}/R_{mother}$, can be determined by Eq. 4.4, which is the function of surface tension coefficient and viscosity. Then, the number of mother and satellite Lagrangian drops is finally computed as

$$n_{drop}\frac{4}{3}\pi R_{mother}^3 + (n_{drop}+1)\frac{4}{3}\pi R_{satellite}^3 = V_{filament}, \tag{4.5}$$

where $V_{filament}$ is the volume of the thin filament that is transferred to the Lagrangian drops in section 4.1. Here, the number of satellite drops is set to $n_{drop}+1$ to satisfy the symmetry condition. First, mother drops are uniformly distributed along the line connecting $\boldsymbol{x}_c$ to $\boldsymbol{x}_{e_1}$ and $\boldsymbol{x}_{e_2}$, where $\boldsymbol{x}_c$, $\boldsymbol{x}_{e_1}$, and $\boldsymbol{x}_{e_2}$ are the center and two end points of the filament that will be transferred to Lagrangian drops. Then, the satellite drops are located at the midpoint between the two mother drops. Figure 6 shows the distribution when $n_{drop} = 2$.

Note that this capillary breakup model does not hold for two-dimensional simulations because there is no capillary breakup mechanisms in two dimensions. For a two-dimensional study, n_{drop} is simply set to 1.

5. Breakup of a round liquid jet by a coaxial flow of gas

When a liquid jet flows in a faster coaxial gas stream, different atomization regimes are observed depending on their Weber numbers and the velocity difference between the liquid and gas (Farago & Chigier 1992). At low gas velocity, a liquid jet wanders in the gas stream inducing bags and rims. At higher gas velocities, the liquid jet is no longer deformed as a whole, but it is peeled off at its surface forming ligaments. These ligaments are broken into small liquid droplets. The typical droplet size is found to decrease with the velocity difference (Lasheras *et al.* 1998; Yatsuyanagi *et al.* 1994). The drop size

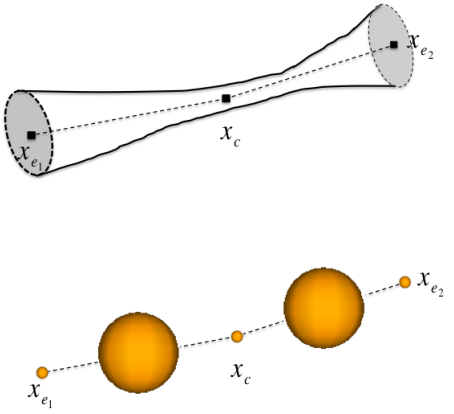

FIGURE 6. Lagrangian mother and satellite drops distribution when $n_{drop} = 2$.

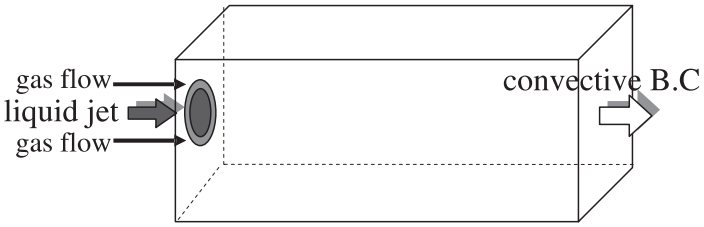

FIGURE 7. Computational domain of a round liquid jet surrounded by coaxial flow of a gas.

distribution shows an exponential tail characteristic of broad size statistics that is very important in industrial applications.

Recently, Marmottant & Villermaux (2004) performed various experiments on the atomization of a liquid jet when a gas stream flows coaxial to its surface. Their experimental findings suggest that two successive instabilities are responsible for the disintegration of the liquid jet into dispersed droplets. First, a Kelvin-Helmholtz type instability triggers axisymmetric modulations on the liquid by shear between the slow liquid and the fast gas stream. Then, these axisymmetric waves undergo transverse azimuthal modulations when the gas velocity is above a critical velocity. This azimuthal secondary instability of the axisymmetric waves was explained by the Rayleigh-Taylor instability in their study. At azimuthal wave crests, liquid ligaments are produced, elongated by the gas stream, and finally broken into droplets.

In this section, we investigate these two instabilities responsible for droplet formation in a round liquid jet and examine the statistical property of the resulting droplets with the Lagrangian drop breakup model.

5.1. *Computational details*

A round liquid jet surrounded by a coaxial flow of gas is simulated as shown in Fig. 7. The liquid jet is injected at the center with the nozzle of diameter D. The surrounding gas flows coaxially with the annular gap thickness h. The gap thickness h is $0.3D$. In this paper, the jet parameters are determined following the experiment of Marmorttant

& Villermaux (Marmottant & Villermaux 2004). The densities of liquid and gas are 998 kg/m^3 and 1.2 kg/m^3, respectively. The Reynolds and Weber numbers of the gas based on the gap thickness h are $Re_g = u_g h/\nu_g = 3770$ and $We_g = \rho_g h u_g^2/\sigma = 34$, respectively, which are the same values as in the experiment. The Reynolds and Weber numbers of the liquid are $Re_l = u_l D/\nu_l = 7137$ and $We_l = \rho_l D u_l^2/\sigma = 100$, respectively, based on the liquid jet velocity and D. The momentum ratio used is $\rho_g u_g^2/\rho_l u_l^2 = 1.14$. An error function is used for the velocity profile of the gas and the liquid at inlets. The inlet boundary-layer thickness of the gas δ_g is $0.04D$ and that of the liquid δ_l is determined by

$$\delta_l = \sqrt{\frac{\mu_l \rho_g}{\mu_g \rho_l}} \delta_g. \tag{5.1}$$

The size of the computational domain used is $-2.5 < x/D < 2.5$, $-2.5 < y/D < 2.5$, and $0 < z/D < 8$. Slip boundary conditions are used except at the jet inlet and exit boundary, and convective boundary conditions are used for the exit boundary. Uniform Cartesian meshes are used for the flow solver and level set solver grids. The grid size for the flow solver is $\Delta x/D = 0.01$. For the level set solver, $\Delta_G/D = 0.01$ is used. The velocity profiles of the gas and the liquid at the inlet are used for the initial velocity field along the jet direction.

5.2. *Kelvin-Helmholtz instability*

Figure 8 shows the axisymmetric modulation on the liquid jet at the initial stage. Two fluids having different velocities are inherently unstable, producing an instability of the Kelvin-Helmholtz type. From the stability analysis by Villermaux (Villermaux 1998), the selected wavelength and frequency at the maximum growth rate are expressed as a function of the density ratio and gas boundary-layer thickness δ_g when a linear velocity profile is assumed (Fig. 9):

$$\lambda_{kh} = \frac{2\pi}{0.8} F(\frac{\rho_l}{\rho_g}) \delta_g, \tag{5.2}$$

where $F(\rho_l/\rho_g)$ is

$$F(\frac{\rho_l}{\rho_g}) = \frac{5}{6} - \frac{1}{6(\rho_l/\rho_g)} + \frac{\sqrt{5 + 13(\rho_l/\rho_g) - 37(\rho_l/\rho_g)^2 + 27(\rho_l/\rho_g)^3}}{6\sqrt{2}(\rho_l/\rho_g)}. \tag{5.3}$$

The group velocity of the most amplified wave number is well estimated by a convection velocity u_c as

$$u_c = \frac{\sqrt{\rho_1} u_1 + \sqrt{\rho_2} u_2}{\sqrt{\rho_1} + \sqrt{\rho_2}}. \tag{5.4}$$

Thus, the period of the surface modulation T_{kh} is given by

$$T_{kh} = \frac{1}{f_{kh}} = \frac{u_c}{\lambda_{kh}}. \tag{5.5}$$

From the computational result, the wavelength is measured as the mean distance between the highest point of the primary waves, and the frequency is measured by calculating the mean velocity of the wave crests. Table 1 shows the wavelength and period divided by those obtained from the stability analysis, respectively. Note that the velocity

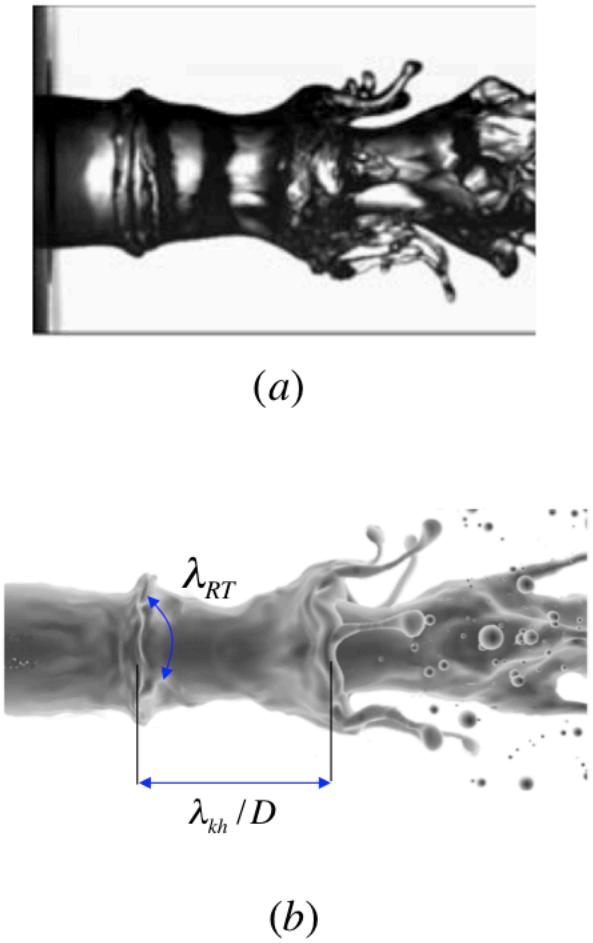

FIGURE 8. Axisymmetric and transverse azimuthal modulations on the liquid surface at the initial stage of the breakup: (*a*) experiment (Marmottant & Villermaux 2004); (*b*) present computation. λ_{kh} and λ_{RT} are the wavelengths of the axisymmetic and azimuthal modulations, respectively.

profile used in the stability analysis is linear. The computed wavelengths are a bit larger than the experiment because the boundary-layer thickness used in this computation is 1.4 times larger than the experiment due to the grid resolution.

5.3. *Ligament development*

After the onset of shear instability causing axisymmetric waves, transverse azimuthal modulations appear, as shown in Fig. 8. Several mechanisms have been suggested to explain these modulations. Villermaux and Clanet Villermaux & Clanet (2002) have proposed that transient acceleration in the direction normal to the liquid at the rims triggers a Rayleigh-Taylor instability, which produces the azimuthal perturbation. The transverse azimuthal modulations grow in amplitude producing small ligaments at the wave crests. Figure 10 shows the formation and development of the ligaments at the

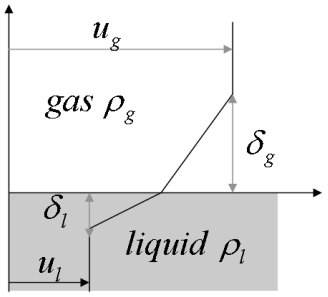

FIGURE 9. Linear velocity profile used in the Kelvin-Helmholtz stability analysis.

TABLE 1. Comparison of the wavelength and period of the primary modulation.

	Experiments (Marmottant *et al.* 2004)	Present study	Stability analysis
Wavelength λ/λ_{kh}	0.29	0.32	1.0
Period T/T_{kh}	0.33	0.35	1.0

wave crests. These ligaments are elongated further by the gas stream and their diameter decreases. Figure 11 shows the snapshot of the phase interface as well as the experimental picture (Marmottant & Villermaux 2004). Five or six ligament structures are observed both in numerical and experimental results. The shape of the phase interface is well matched with the experimental observation qualitatively, as shown in Fig. 11.

5.4. *Subgrid capillary breakup model for ligament breakup*

The ligaments are finally pinched off and broken into liquid droplets. When the ligaments are detached, a capillary instability grows in a very short time that results in several droplets of different sizes. In the experiment, the smallest ligament size before breakup is about $\xi_b/D \sim 0.025$, while the G grid size is $\Delta_G/D = 0.01$ in the present simulation. Thus, the breakup length scale ξ_b is not fully resolved because at least 4 or 6 grid points are needed to resolve the breakup of the ligament. Thus, the subgrid capillary breakup model is used to predict subgrid drops, which are inserted as Lagrangian drops.

Figure 12 shows the ligament breakup process with the subgrid capillary breakup model. Figure 12 (a) shows the thin ligament tracked by the level set method before breakup. When it satisfies the breakup criterion specified in section 4.2, it is replaced by Lagrangian drops as in Fig. 12 (b). The number and size of drops are calculated by the capillary instability theory as explained in section 4.3.

5.5. *Drop formation*

Several drops are formed from the detached ligaments. In natural spray formation, drops, such as rain drops and fuel droplets, have a broad range of sizes. The statistical drop size distribution has been known to show an exponential tail shape. In the computational simulations, subgrid liquid drops smaller than the G-grid resolution are predicted by the subgrid capillary breakup model. Figure 13 shows the drop size distribution as well as

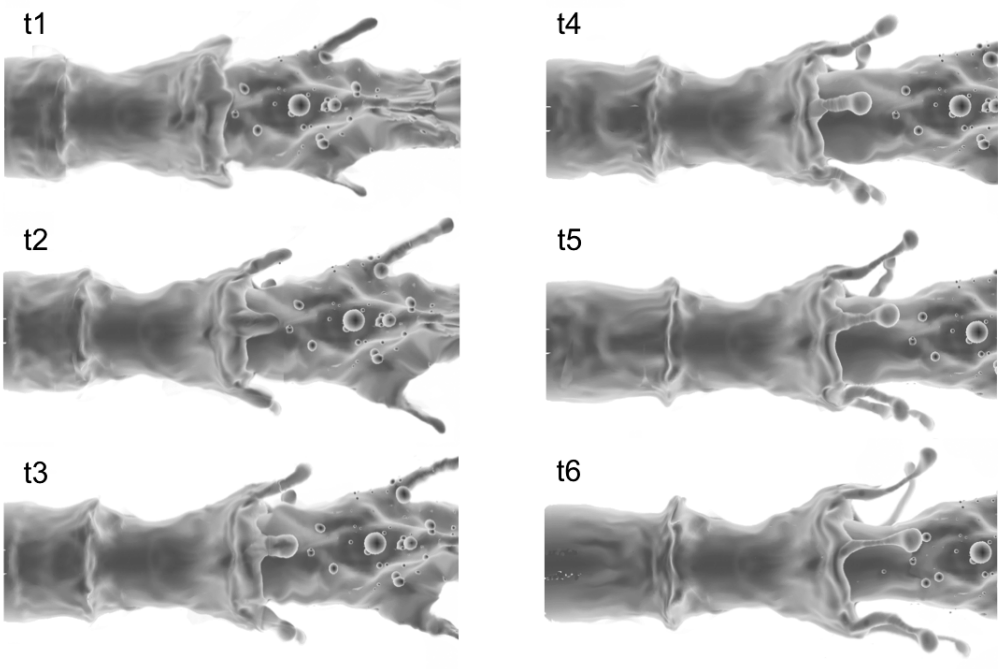

FIGURE 10. Development of the ligaments from the azimuthal perturbations.

experimental result (Marmottant & Villermaux 2004). Here, the coarse grid numerical simulation of $\Delta/D{=}\Delta_G/D = 0.02$ is performed to study the grid resolution effect on the drop size distribution. As shown in Fig. 13, the number of small subgrid liquid drops is slightly over predicted for both grids compared to the experiment, however, the drop size distributions at resolved scales show good agreement with the experimental measurement. The possible reason for discrepancy in small scales is that experimental measurement in counting drops might have larger errors at smaller scales and evaporation can also occur on small sprays, although evaporation is neglected in the present simulation. Without the subgrid capillary breakup model, all subgrid drops are not captured. The loss of small drops can cause serious errors in predicting combustion phenomenon especially in simulations of liquid fuel combustion.

6. Conclusions

An accurate and robust numerical method has been developed to simulate the whole atomization process of liquid jet. The phase interface is tracked by the level-set method to capture frequent topological changes due to breaking or merging. Because of the broad-band characteristics of length scales in two-phase flow, a Lagrangian drop breakup model has been developed, which is coupled to the level-set method. In this approach, small subgrid droplets produced from resolved ligaments are then transferred from the level-set representation to the Lagrangian particles. The further secondary atomization is handled by a stochastic breakup model. When pinching-off of ligaments is not resolved on the level-set grid, a capillary breakup model is used to predict the drop size distribution from the pinching off and inserted as Lagrangian drops. This method improves the mass conservation as well as reducing the computational cost.

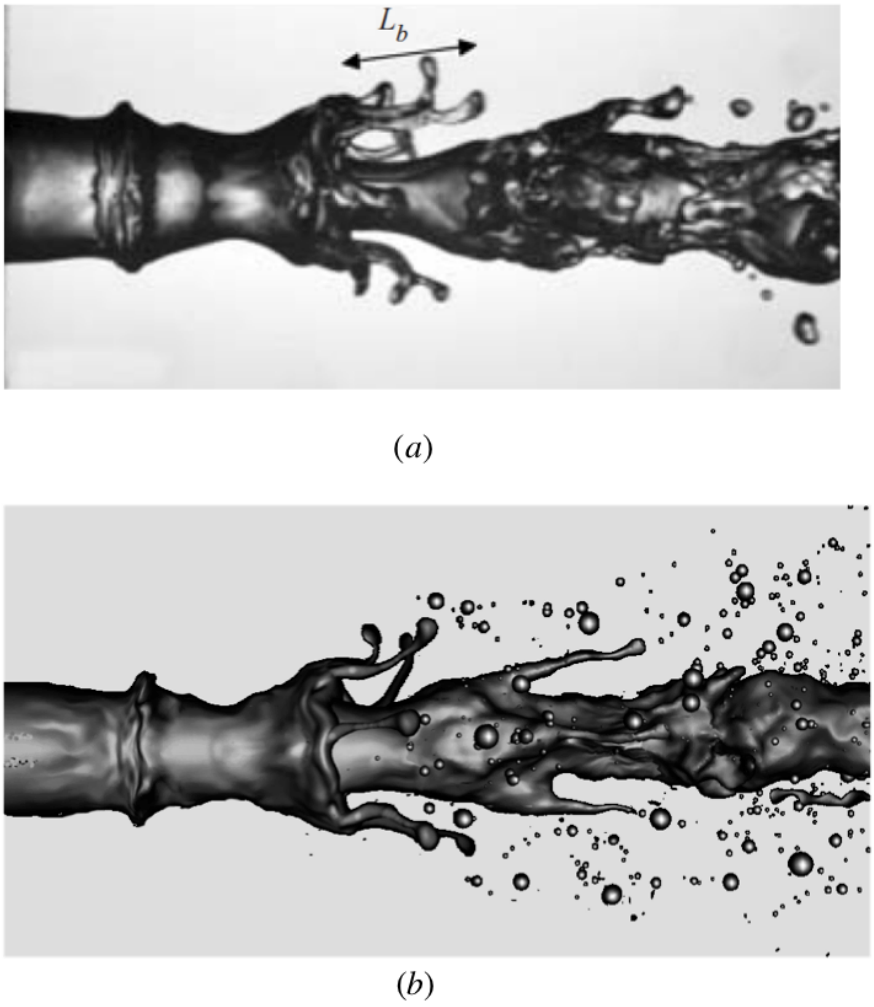

FIGURE 11. Instantaneous snapshot of the phase interface: (a) experiment (Marmottant & Villermaux 2004); (b) present computation.

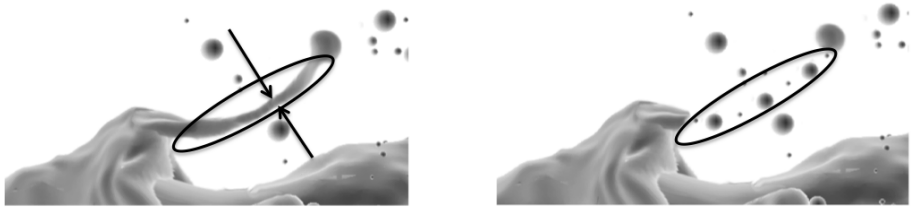

FIGURE 12. (*a*) Ligaments tracked by the level-set method before breakup; (*b*) formation of Lagrangian spherical droplets from the ligaments.

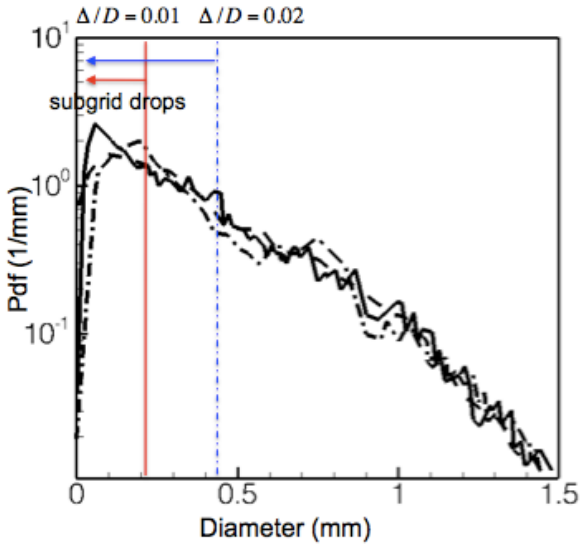

FIGURE 13. Drop size distribution compared with the experimental result: ——, $\Delta/D = \Delta_G/D = 0.01$; −·−·−, $\Delta/D = \Delta_G/D = 0.02$; − − −, experimental measurement (Marmottant & Villermaux 2004).

In order to show the capability of the method as an efficient tool in the breakup process, the atomization of a round liquid jet surrounded by a coaxial gas is considered. The numerical results are consistent with the observed breakup mechanisms in the experiment and the stability analysis. The drop size distribution of the resulting spray after breakup is also compared with the experimental data. The subgrid drops are also predicted by the Lagrangian drop breakup model, which shows the applicability of our method for numerical simulation of the atomization process.

Acknowledgments

The authors thank Marcus Herrmann and Frank Ham for discussions and helpful advice. The work presented in this paper was supported by the Office of Naval Research.

REFERENCES

APTE, S. V., GOROKHOVSKI, M. & MOIN, P. 2003 Les of atomizing spray with stochastic modeling of secondary breakup. *Int. J. Mult. Flow* **29**, 1503–1522.

CHANDRASEKHAR, S. 1981 *Introduction to hydrodynamic stability*. Cambridge University Press.

CROWE, C., SOMMERFELD, M. & TSUJU, Y. 1998 *Multiphase flows with Droplets and Particles*. CRC Press, Boca Ranton, FL.

FARAGO, Z. & CHIGIER, N. 1992 Morphological classification of disintegration of round liquid jets in a coaxial air stream. *Atomization and Sprays* **2**, 137–153.

HAM, F. & IACCARINO, G. 2004 Energy conservation in collocated discretization schemes on unstructured meshes. *Annu. Res. Briefs* **2004**, 3–14.

Herrmann, M. 2005 Refined level set grid method for tracking interfaces. *Annu. Res. Briefs* **2005**, 3–18.

Herrmann, M. 2008 A balanced force refined level set grid method for two-phase flows on unstructured flow solver grids. *J. Comput. Phys.* **227**, 2674–2706.

Kim, D. & Moin, P. 2011 Direct numerical simulation of two-phase flows with application to air layer drag reduction. *Report No. TF-125, 2001, Stanford University* .

Lasheras, J. C., Villermaux, E. & Hopfinger, E. J. 1998 Break-up and atomization of a round water jet by a high-speed annular air jet. *J. Fluid Mech.* **357**, 351–379.

Mahesh, K., Constantinescu, G. & Moin, P. 2004 A numerical method for large eddy simulation in complex geometries. *J. Comput. Phys.* **197**, 215–240.

Marmottant, P. & Villermaux, E. 2004 On spray formation. *J. Fluid Mech.* **498**, 73–111.

Pierce, C. & Moin, P. 2001 Progress variable approach for large-eddy simulation of turbulent combustions. *Report No. TF-80, 2001, Stanford University* .

Rayleigh, L. 1878 On the instability of jets. *Proc. Lond. Math. Soc.* **10**, 4–13.

Reitz, R. D. 1987 Modeling atomization processes in high-pressure vaporizing sprays. *Atomization Spray Tech.* **3**, 309–337.

Rutland, D. F. & Jameson, G. J. 1970 Theoretical prediction of the sizes of drops formed in the breakup of capillary jets. *Chem. Eng. Sci.* **25** (11), 1689 – 1698.

Tanner, F. 2004 Development and validation of a cascade atomization and drop breakup model for high-velocity dense sprays. *Atomization and Sprays.* **164**, 211–242.

Villermaux, E. 1998 On the role of viscosity in shear instabilities. *Phys. Fluids* **10**, 368–373.

Villermaux, E. & Clanet, C. 2002 Life of a flapping liquid sheet. *J. Fluid Mech.* **462**, 341–363.

Yatsuyanagi, N., Sakamoto, H. & Sato, K. 1994 Atomization characteristics of liquid jets injected into a high-velocity flow field. *Atomization and Sprays* **4**, 451–471.

Yuen, M.-C. 1968 Non-linear capillary instability of a liquid jet. *J. Fluid Mech.* **33** (01), 151–163.